# Examination of spaceborne imaging spectroscopy data utility for stratigraphic and lithologic mapping

**Alon Dadon,[a] Eyal Ben-Dor,[b] Michael Beyth,[c] and Arnon Karnieli[a]**
[a] The Remote Sensing Laboratory, Jacob Blaustein Institutes for Desert Research, Ben-Gurion University of the Negev, Sede-Boker Campus 84990, Israel
[b] The Remote Sensing and GIS laboratory, Geography and Human Environment Department, Tel-Aviv University, Israel
[c] Geological Survey of Israel, Jerusalem, Israel
Address all correspondence to: Arnon Karnieli, The Remote Sensing Laboratory, Jacob Blaustein Institutes for Desert Research, Ben-Gurion University of the Negev, Sede-Boker Campus 84990, Israel. Tel: 972 8 6596855; Fax: 972 8 6596805; E-mail: karnieli@bgu.ac.il

**Abstract.** Due to the increasing development of image spectroscopy techniques, airborne and spaceborne hyperspectral images have in recent years become readily available for use in geological applications. One of the prominent advantages of imaging spectroscopy is its high spectral resolution, producing detailed spectral information in each pixel. The current study aims at exploring the feasibility of the Earth-Observing-1 Hyperion imaging spectrometer to map the geology arena over the Dana Geology National Park, Jordan. After overcoming the common preprocessing difficulties (e.g., smile effect), a classification scheme of two levels was applied. The first level resulted in a stratigraphic classification product of eleven classes and the second level in a lithologic classification product of six classes. The overall accuracy of the stratigraphic product was 57%, while that of the lithologic product was 79%. Mismatches in classification were mostly related to terrestrial cover of the lower topography formation by rock and sand debris. In addition, low accuracy values can be attributed to Hyperion's high sensitivity, leading to recognition of different mineral compositions as different classes within a rock formation, while the conventional geology-stratigraphic map generalizes these different classes into one formation. The methods practiced in the current research can advance the Hyperion's classification capabilities and therefore can be applied in different geological settings and additional disciplines such as penology, agriculture, ecology, forestry, urban, and other environmental studies.  [DOI: 10.1117/1.3553234]

**Keywords:** hyperion; geology; stratigraphic mapping; lithologic mapping; classification; accuracy assessment.

Paper 10043R received Mar. 24, 2010; revised manuscript received Oct. 28, 2010; accepted for publication Dec. 20, 2010; published online Mar. 16, 2011.

## 1 Introduction

Different geological and pedological formations are distinguished mainly according to their mineral composition, weathering characteristics, and landforms. Therefore, geological mapping and mineral exploration are primarily based on chemical and physical properties of rocks and soils. Field geologists face obstacles such as accessibility and inability to detect subtle changes in mineral composition in order to determine the spatial distribution of different rock units. Remote sensing applied for geological research enables a wide view of the research site along with a spectral dimension of the observed surface and therefore offers obvious advantages for geosciences. Since chemical and physical properties can be identified by imaging spectroscopy,

1931-3195/2011/$25.00 © 2011 SPIE

geology is an attractive discipline for utilizing this technology. Several early studies reported successful identification of various minerals and showed to some extent their distribution at the field sites.[1–12] Following these achievements, in November 2000 NASA launched the first hyperspectral spaceborne system named Earth-Observing-1 (EO-1) Hyperion. Hyperion is a pushbroom (forward scanning) imaging spectrometer covering the 0.4 to 2.5 $\mu$m spectral region with a 30 m spatial resolution and a 7.7 km swath.[13] As opposed to the common operated multispectral spaceborne sensors that have only four to seven spectral bands, the Hyperion has 242 bands with approximately 10 nm bandwidth for each one. Observing ground features from space with high spectral resolution on a regional scale is a great challenge for earth scientists, even though the Hyperion system has several notable drawbacks. Due to the limitations of the pushbroom technology, uncalibrated detectors leave a vertical "stripe" in the image band. Another malfunction of the Hyperion sensor is the curvature effect shifting the exact position of both dimensions (spectral and spatial across the image).[14] To overcome these drawbacks and obtain useful reflectance data, a preprocessing stage is required, which includes depletion of atmospheric noise as well as the artifacts caused by the sensor and its electro-optic characteristics.

Early results from selected Hyperion validation sites show that the system generally performs correctly and produces useful geologic (mineralogy/lithology) information.[5,13,15–22] However studies comparing Hyperion to hyperspectral airborne sensors pointed out several limitations in the data achieved by the former. One limitation is the reduced spatial resolution (30 versus 2–20 m in the space versus airborne systems, respectively), and another are the lower signal to noise ratio[23] values (50:1 versus $>$500:1 and more) resulting in limited detection capability of similar fine spectral details.[5,16,22,23] Furthermore, Hyperion data acquired under less than optimum conditions (winter season, dark targets) have even lower Short Wave Infrared (SWIR) SNR, allowing only the mapping of the most basic mineral occurrences.[23]

The main objective of the current research is to explore the potential of EO-1 Hyperion data, despite the noted limitations, for geologic mapping. Specifically, the study aimed at separately classifying the research site at stratigraphic and litological levels.

## 2 Methodology

### 2.1 *Research area and geologic background*

The research site lies mainly within the borders of the Dana Geology National Park, located in south-west Jordan (035º18′30″ E 030º40′50″ N). The site is located at the eastern edge of the Dead Sea Transform and the desert lowlands of the Arava valley (Fig. 1). The region is characterized by a hyper arid climate with an annual average rainfall of 50 mm. Low vegetation cover results in an exposed lithology. Topography is generally flat to moderate. The tectonic regime is mainly controlled by the NNE Dead sea transform.[24–28] Geology in the area ranges from Precambrian to Quaternary in age including both sedimentary and igneous rock types. The igneous rocks are predominantly Precambrian and include a variety of late proterozoic granitoids (Syenigranite to Granodiorite) including the Finan granite (FN), Minshar monzogranite (MM), Hunayk monzogranite/ Urf porphyry (HK) As-Sadrra granodiorite (AS), and volcanic rocks of the Ghuwayr volcanic suite (GR) consisting of basic green tuffs, pyroclastic fragments, and basaltic lava. Sedimentary rocks include Cambrian massive Salib arkosic sandstone formation (SB), Burj dolomite-shel formation (BDS), Umm Ishrin sandstone (IN) of late-middle Cambrian, as well the lower cretaceous Kurnub sandstone group (KS) overlain by upper Cretaceous Naur limestone (NL). A variety of superficial deposits cover extensive areas in the research site (defined herein as PAl), these include alluvium and wadi sediments (Al), Pleistocene conglomerate (Plg), alluvial fans, fluviatile gravel, as well as sand and sand dunes (Als).[29,30] Various clay minerals and alteration minerals including ferric oxides and hydrothermal alteration associated minerals (sericite, goethite, and hematite) occur in the area.[31] In fact the area was a major copper mining center during the late Neolithic period to the medieval times. The remains of the Finan village and of the mines can still be found in the southern part of the reserve.[32]

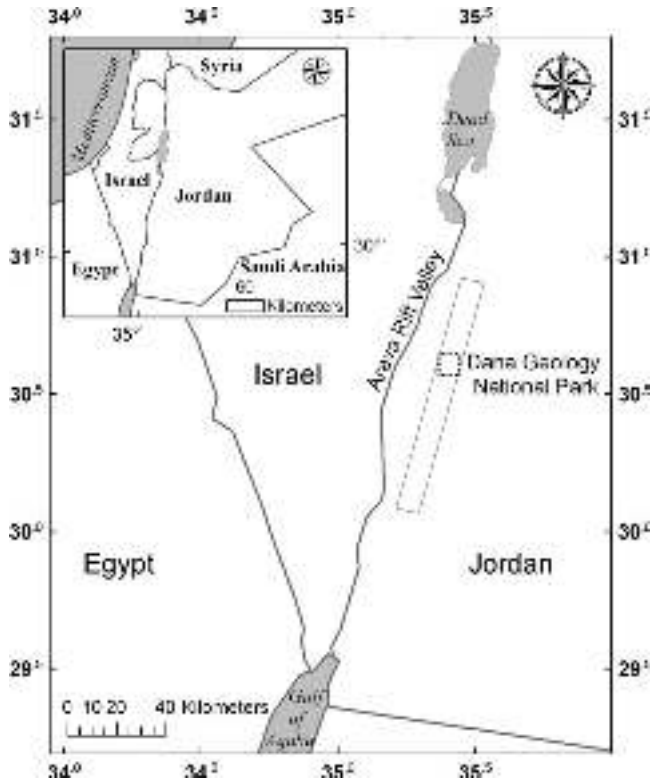


**Fig. 1** Study area showing the Hyperion flightline and the research site at the Dana Geology National Park, Jordan.

The stratigraphy of the park was mapped by Rabba[29] and the lithology, mineralogy, and land forms are well documented.[27,28,33–35] Previous remote sensing-based geological surveys of the site were performed by Kaufmann[36] and Abdelhamid and Rabba,[30] utilizing Landsat multispectral data. To conclude, the arid conditions, diverse lithology, mineralogy assemblage, and the accumulated past research data make the Dana Geology National Park an attractive research site for remote sensing of surface geology using the hyperspectral technology.

## 2.2 *Preprocessing methods*

A Level 1B Hyperion image [raw digital numbers (DN)] acquired over the research area was used for this study. A flowchart describing the preprocessing of the raw data along with the processing procedures is presented in Fig. 2.

The radiometric calibration was carried out according to the Hyperion user guide (http://eo1.usgs.gov/userGuide/index.html), resulting in a radiance dataset with 198 calibrated radiance bands. The first and last columns of each band image were omitted due to miss calibration. Noise reduction operations were applied, in order to remove artifacts related to striping and other factors, to improve data signal to noise ratio[16,22,23,37,38] (SNR). The striping effect (bad pixels), resulting from the Hyperion pushbroom system, was corrected by using the nearest neighbor algorithm local destriping approach.[14,16,39] Minimum noise fraction (MNF) transformation was applied to segregate noise from the data.[40] Trend line smile correction[41] (TLSC) was used for correcting the smile. TLSC is an image-based method utilizing atmospheric gas absorptions (specifically their derivative values) to recognize the smile appearing in the image and then correct it using MNF. The correction includes validation according to MODTRAN data.[42] The output radiance values from the above procedure still include path

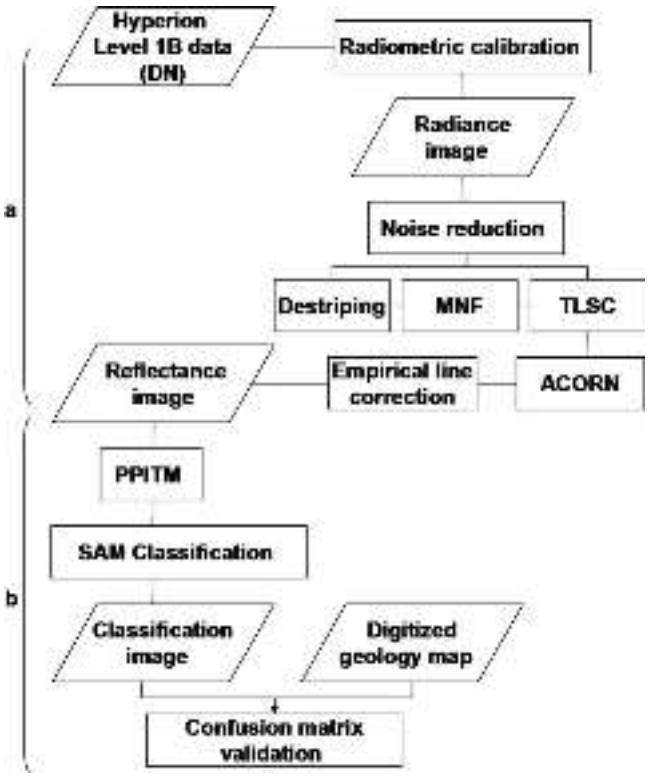


**Fig. 2** Methodology flowchart. (a) Preprocessing procedures; (b) classification and validation procedures.

radiance artifacts. These were removed by the atmospheric correction now (ACORN) code.[43] Ground truth samples, which included different land covers and surface components of several rock types, were measured using an Analytical Spectrometer Devices (ASD) field spectrometer[44] both in the field and in the laboratory. The empirical line (EL) technique,[45] based on selected spectra, was used for refining the atmospheric correction. Through the EL calibration process the image spectra is forced to match reflectance spectra collected from the field, using dark and bright targets. The targets selected for the EL correction were chosen mainly according to their cross track location and spectral albedo. The bright target chosen was sand (Als), and the dark one was FN. Both were collected from homogeneous areas. The final output product of this stage was a noise-reduced reflectance Hyperion image.

To assess the effect of the preprocessing methodology on noise in the data, SNR (Refs. 37–39 and 46) was calculated by computing the coefficient of variation (ratio between the standard deviation and the mean) of the signals along three cross sections over homogeneous areas.[39–41,48] SNR calculations were applied separately for the visible (VIS), near infrared (NIR), and SWIR spectral regions (Table 1). Results presented in Table 1 demonstrate an increase in visible-Near Infrared (VNIR) SNR values from 25 for the initial radiance image up to 110 in the noise-reduced reflectance image. For the SWIR region, SNR at the shorter wavelength values rise from a level of 30–40 to approximately 100 and at the longer ones an improvement from around 20 to 60 SNR values is shown. The highest increase in SNR is evident on the right side of the image, achieving a five-fold improvement. This improvement is ascribed to the correction of the smile effect mainly observed on the right side of the dataset.

Validation of the final reflectance signals was performed by comparing specific spectra extracted by the ASD to those acquired over known homogeneous areas by the Hyperion. ASD spectra were resampled according to Hyperion spectral configuration in order to enable the comparison. Figure 3 shows a comparison between the spectra of field samples and spectra of

**Table 1** Signal to noise ratio (SNR) values for different spectral regions over three areas of the image. Calculations appear for the radiance image, for the reflectance image, and for the final corrected and noise reduced image.

| Image Type | SNR | | | |
|---|---|---|---|---|
| 427–702 nm | Left | Middle | Right | Mean |
| Radiance | 56 | 59.1 | 23.7 | 46.3 |
| Reflectance | 43.4 | 16.8 | 48.7 | 36.3 |
| Final | 90.1 | 108.3 | 110.6 | 103 |
| 1003–1608 nm | Left | Middle | Right | Mean |
| Radiance | 35.1 | 34.1 | 17.5 | 28.9 |
| Reflectance | 37.27258 | 15.73864 | 36.92807 | 30 |
| Final | 100.6 | 93.8 | 101.4 | 98.6 |
| 2002–2395 nm | Left | Middle | Right | Mean |
| Radiance | 28.2 | 23.6 | 17.6 | 23.2 |
| Reflectance | 28.2 | 13.7 | 23.6 | 21.8 |
| Final | 70.9 | 48.7 | 67.5 | 62.4 |

selected image pixels where similarity is well presented for FN, Als, HK/ Urf porphyry, and MM [Figs. 3(a)–3(d), respectively]. These findings confirm noise removal and credibility of the reflectance Hyperion image.

## 2.3 *Classification*

Having confirmed the success of the preprocessing scheme, the Hyperion reflectance image was subjected to processing stages of classification and validation. An area of interest of about 7 $km^2$, containing representative rock units, was selected for detailed processing. To differentiate rock formations within the research area, several classification methods, embedded in the environment for visualizing images (ENVI) software, were applied. Pixel purity index (PPI) was used to find the most "spectrally pure" pixels (endmembers) in the image. These were then grouped into several classes, based on their spectrum characteristics, and introduced into the spectral angle mapper (SAM) supervised classification method[47–49] implemented in ENVI image analysis software. SAM generates an n-dimensional feature vector, with n being the

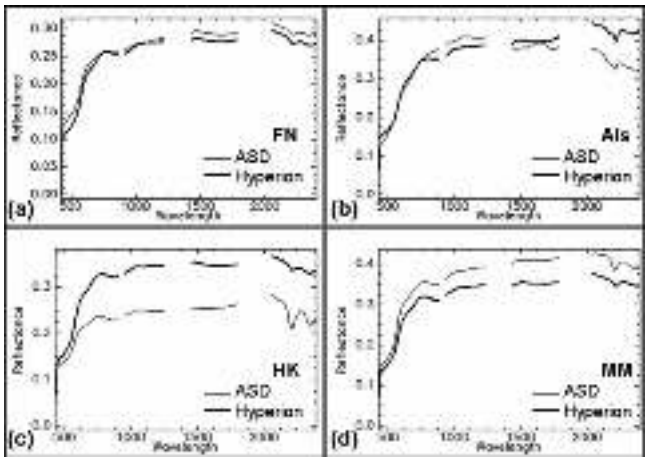


**Fig. 3** Spectral measurements of field samples in comparison to spectra of selected Hyperion pixels. (a) FN, (b) Als, (c) HK/ Urf Porphyry, and (d) MM.

number of spectral bands, using the vector angles to match pixels with the endmembers. Being dependent on the direction (angle) and not on the length of the spectral vector, this technique is relatively insensitive to illumination and albedo effects.[50] A classification scheme of two levels, for stratigraphic and for lithologic mapping, was applied. The first level includes eleven classes and the second includes six classes. A geologic (stratigraphic) map in a scale of 1:50,000 (Ref. 32) was later used as a reference for validating the classification results.

### 2.4 *Accuracy assessment*

The accuracy assessment of the final classification products was performed according to the error matrix method using randomly selected pixels.[51–53] Errors of exclusion (omission) represent pixels that belong to the ground truth class but the classification technique failed to classify them into the proper class. The user accuracy is defined as the probability that a pixel classified as a particular feature in the image is actually that feature.[51] Errors of inclusion (commission) represent pixels that belong to another class but are labeled as belonging to the class of interest. Dividing the total number of correct pixels in a category by the total number of pixels that were classified to that category provides the "user's accuracy" that means the probability that a pixel classified in the image actually represents that category on the ground. Another technique used for accuracy assessment is called Kappa coefficient.[54] This index compares the results of an image classification to the results of a random classification. The possible values of the Kappa coefficients range from $+1$ (perfect agreement) via 0 (no agreement above that expected by chance) to $-1$ (complete disagreement). The above accuracy procedures were implemented in ENVI.

## 3 Results and Discussion

### 3.1 *Stratigraphic information extraction*

A stratigraphic map is one of the most common products of geologic mapping. It shows the distribution, configuration, or aspect of geological units exposed at the surface according to their age and composition. Nevertheless, each of the stratigraphic units may vary in its composition and may even include several rock types. Moreover, it is not always possible to properly map stratigraphic contour lines as happens in cases where the strata are extremely fractured, mixed, discontinued, or covered (e.g., by superficial deposits). These factors most likely add to the complexity of producing a remotely sensed geology product, moreover when using imagine spectroscopy that is highly sensitive to composition changes. Yet, taking advantage of the preprocessing procedure that results in an improved image, the SAM classification of the processed data was able to detect all eleven rock units represented in the traditional geologic (stratigraphic) map of the research area [Figs. 4(a) and 4(b)].

Accuracy of the Hyperion stratigraphic classification product was assessed according to the error matrix method using the 1:50000 geologic (stratigraphic) map as a reference. The overall accuracy according to 102,902 randomly selected pixels was 57% with 0.45 Kappa Coefficient (Table 2).

The error matrix presented in Table 2 suggests overlapping in several neighboring rock units. One case is the NL and KS formations, having high mutual errors of confusion (Table 2) and virtually opposite omission and commission values (Table 3). Other than spectral similarity, this confusion is mainly attributed to talus superficial deposits due to the relatively prominent topography of the NL formation. Mixed pixels at the boundary of these layers contribute to errors of omission and commission. In the original geologic (stratigraphic) map most of the contour lines of AS and MM formations are marked with dashed lines, indicating unclear boundaries. The reason for this is that AS and MM are located at relatively low topography and intersected by wadis (dry river valleys) comprising sand dunes (Plc), alluvium, wadi sediments (Al), as well as

**Table 2** Error matrix (percentages) of the stratigraphic classification product.

| Class | NL | GR | SB | AS | MM | BDS | IN | KS | HK | FN | PAI | User's Accuracy (%) |
|---|---|---|---|---|---|---|---|---|---|---|---|---|
| NL | **64.10** | 0.31 | 0.75 | 0.62 | 4.35 | 3.28 | 5.27 | 39.06 | 0.06 | 1.07 | 4.28 | 44.72 |
| GR | 0.47 | **85.69** | 0.00 | 0.82 | 0.07 | 0.00 | 0.00 | 0.00 | 0.02 | 0.00 | 0.71 | 75.99 |
| SB | 1.11 | 0.00 | **61.52** | 0.00 | 3.02 | 44.04 | 3.15 | 0.64 | 6.10 | 4.36 | 5.39 | 28.01 |
| AS | 0.07 | 6.92 | 0.00 | **39.48** | 1.00 | 0.00 | 0.00 | 0.00 | 8.44 | 0.03 | 0.95 | 22.87 |
| MM | 0.20 | 0.15 | 0.23 | 2.06 | **14.92** | 1.60 | 10.87 | 0.01 | 10.07 | 11.52 | 1.07 | 17.98 |
| BDS | 0.36 | 0.08 | 21.86 | 0.00 | 3.14 | **27.62** | 0.61 | 0.45 | 4.23 | 10.31 | 1.84 | 36.66 |
| IN | 1.18 | 0.00 | 0.40 | 0.00 | 0.21 | 3.52 | **53.82** | 5.81 | 0.00 | 0.23 | 2.14 | 60.81 |
| Ks | 23.61 | 0.00 | 0.75 | 0.00 | 0.81 | 1.28 | 0.65 | **39.31** | 0.01 | 0.09 | 1.18 | 63.8 |
| Hk | 0.00 | 2.92 | 3.71 | 22.68 | 35.28 | 3.49 | 3.11 | 0.35 | **47.72** | 43.49 | 3.87 | 38.36 |
| FN | 0.00 | 0.00 | 0.45 | 2.58 | 0.86 | 0.72 | 1.48 | 0.00 | 3.54 | **13.00** | 0.20 | 59.15 |
| PAI | 8.88 | 3.92 | 10.34 | 31.75 | 36.35 | 14.44 | 21.05 | 14.37 | 19.83 | 15.91 | **78.36** | 75.91 |
| Overall accuracy | (58410/102902) | 56.76% | | | | | | | | | | |
| Kappa coefficient | 0.45 | | | | | | | | | | | |

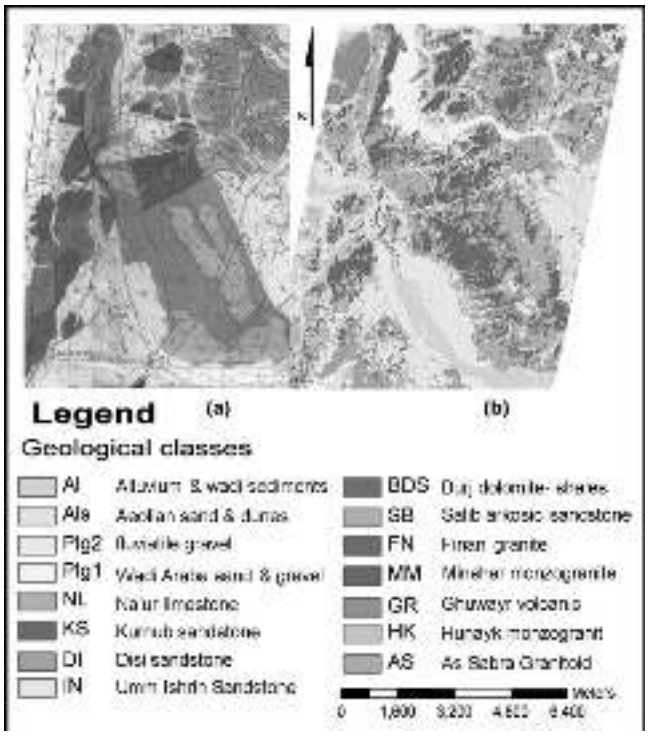


**Fig. 4** (a) Geological map of the research area originally at 1:50,000 scale (after Rabba, 1991). (b) Stratigraphic product result of the SAM classification.

Pleistocene conglomerate (Plg). Therefore, it is difficult to identify the spatial boundaries of these formations. Moreover, alluvial and particularly eolian superficial deposits are relatively dynamic and quickly change in space and time. Hyperion classification results display these difficulties. Consequently, AS and MM formations have low user accuracy (23 and 18%, respectively) and a relatively high superficial deposits omission (32 and 36%, respectively) (Table 3).

Finan granitic (FN) formation, on the other hand, is located at higher topography, and borders with superficial deposits (alluvial sand) only at limited sites. Nevertheless, its stratigraphic classification accuracy stands only at 59% (Table 2) with omission values as high as 87% (Table 3). A closer look at the stratigraphic error matrix (Table 2) also shows that most of these incompatibilities are found within the HK and MM units and appear spatially in the distribution area of the FN formation (Fig. 3). The FN unit is mainly composed of aplite granite, quartz porphyry, and syeno-granite[33] and is predominantly rich with clay minerals of varying

**Table 3** Errors of commission and omission of the stratigraphic classification product.

| Class | Commission (%) | Omission (%) |
|---|---|---|
| NL | 55.28 | 35.90 |
| GR | 24.01 | 14.31 |
| SB | 71.99 | 38.48 |
| AS | 77.13 | 60.52 |
| MM | 82.02 | 85.08 |
| BDS | 63.34 | 72.38 |
| IN | 39.19 | 46.18 |
| KS | 36.20 | 60.69 |
| HK | 61.64 | 52.28 |
| FN | 40.85 | 87.00 |
| Als | 24.09 | 21.64 |

compositions, while Hunayk monzogranite / Urf porphyry (HK) and Minshar Monzogranite (MM) are similar and are characteristically more felsic with higher biotite content. Due to Hyperion's high spectral resolution and in spite of their spectral similarity, FN, MM, and HK granites were successfully classified and located in different sites of the research area. Nevertheless, as noted from the high omission values of FN (Table 3), most misclassified MM and HK pixels appeared within the spatial distribution of FN stratigraphic units due to similar mineral compositions resulting in similar spectral signatures. Note that while areas of subtle mineral composition variation within stratigraphic rock formations (e.g., chemically weathered areas) are not defined in the generalized stratigraphic division of the conventional map, they are recognized by Hyperion and may cause classification incompatibilities.

SB and BDS neighboring units present low user accuracy (28% and 36%, respectively). Their settings are a combination of moderate topography, limited spatial distribution, and undefined borders. GR and IN, on the other hand, are spatially distributed in distinct sites of the research area having low mixed pixels and therefore relatively high user accuracies (76% and 61%, respectively).

## 3.2 *Lithologic classification*

The 1:50,000 geology (stratigraphic) map was generalized into a lithologic map where six lithology classes were defined for both igneous and sedimentary rock types. Igneous rocks present at the site are volcanic rocks comprising Ghuwayr volcanic suite (GR) as well as plutonic rocks (Pl) comprising FN, MM, and HK formations. As-Sadra granodiorite (AS) is the oldest least exposed plutonic rock in the research site and is therefore considered as an outlier. The main sedimentary rocks are Sandstone (S) comprising KS and IN formations; sandstone, conglomerate and dolomite-shale (SCD) comprising BDS and SB formations; and Naur limestone (NL). Hyperion SAM classification detected all six lithologic units appearing in the research site (Fig. 5). While the classification results [Fig. 5(b)] are visually compatible with the lithologic map [Fig. 5(a)], it is clear where ground truth verification points are needed for validating the analysis. This however, requires a comprehensive field study that was out of the scope of this study. Therefore, the lithologic map was used as reference for validation.

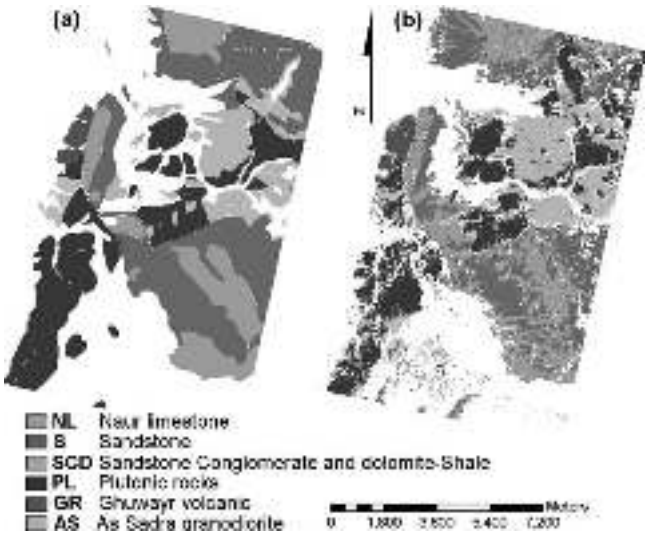


**Fig. 5** (a) Geological (lithologic) map of the research area originally at 1:50,000 scale (after Rabba, 1991). (b) Stratigraphic product result of the SAM classification.

**Table 4** Error matrix (pixels) of the lithologic classification product.

| | Sedimentary | | | | Igneous | | User's |
|---|---|---|---|---|---|---|---|
| **Classification** | **NL** | **SCD** | **S** | **PI** | **GR** | **AS** | **Accuracy (%)** |
| NL | **94.84** | 2.39 | 9.29 | 1.49 | 0.32 | 0.88 | 88.62 |
| SCD | 2.45 | **85.63** | 6.17 | 16.37 | 0.56 | 0.00 | 70.56 |
| S | 1.59 | 4.41 | **55.36** | 0.16 | 0.00 | 0.00 | 86.89 |
| PI | 0.61 | 7.54 | 29.18 | **75.93** | 3.60 | 42.23 | 79.72 |
| GR | 0.40 | 0.02 | 0.00 | 0.17 | **86.41** | 3.67 | 92.31 |
| AS | 0.10 | 0.01 | 0.00 | 5.87 | 9.11 | **53.23** | 25.65 |
| Overall accuracy | (33457/42542) | 78.64% | | | | | |
| Kappa coefficient | 0.7147 | | | | | | |

Accuracy assessment of the lithologic classification product was performed using 42,542 randomly selected pixels. The overall accuracy of the lithologic classification product was 79% with a Kappa coefficient of 0.71 (Table 4). The sedimentary rocks were identified with a user accuracy of 82%, and the Igneous rocks with user accuracy of 86%, excluding AS that has a low matching accuracy of 25% and therefore is considered as an outlier. This is due to the limited exposed area of AS rocks in the research site as noted in Sec. 3.1.

## 4 Summary and Conclusions

Although the Hyperion raw data was found to be noisy (mostly comprising arrays related to the pushbroom system) we were able to generate reasonable reflectance information that enabled a detailed classification process of the rocks and the land formations within the research area.

Validation according to reference geologic (stratigraphic/lithologic) maps enables independent random sampling of a high number of points (pixels). This comprehensive sampling scheme would not be possible by means of limited field sampling. Therefore, the proposed validation scheme is generally recommended as a preferred one and not only for accessibility limited sites.

When comparing the classification products to a standard geologic (stratigraphic) map, it is important to note that conventional geology mapping relies on our ability to generalize rock units and their boundaries in the field. However, Hyperion's high sensitivity to spectral changes may be over sensitive to classify the stratigraphic unit as one generalized homogeneous formation. Therefore, different mineral compositions within a stratum will appear as different classes, while the conventional geology-stratigraphic map generalizes these changes. A lithologic map, on the other hand, mainly accounts for the rock type. Therefore, when generalization is applied to the hyperspectral classification product as well as to the stratigraphic units of the map in the process of configuration of a lithologic map, the results significantly improve both for statistical reasons (fewer classes) and for spectral reasons (generalization of composition difference). Moreover, conventional mapping considerations rely on interpretation of stratigraphic relations combined with other preliminary information such as drill holes and cross sections. Such interpretation was not added to the classification products in the current research and may be considered for further research of geodata modeling and mapping. Considering these restrictions, the lithologic classification product was found to be satisfactory. However, the ability of Hyperion data to provide a standalone stratigraphic product was found to be limited, although it comprises detailed information that may contribute much to the definition of serigraphic rock units.

To conclude, properly processed and interpreted spaceborne hyperspectral imagery can be an effective tool for lithologic mapping and might provide accurate information to support geology (stratigraphic) mapping, especially in arid environments. The improved classification results are mainly ascribed to the methodology practiced in the current research, improving Hyperion's image SNR by up to five fold. This significantly reduces misclassifications related to sensor and path radiance noise.[41] It is therefore believed that the methods practiced in the current research

for processing Hyperion data and the applicable scheme presented for validation of hyperspectral classification results may be further applied, with minor modifications, in other disciplines (such as soil, vegetation, water, ecology, environmental studies, and more), incorporating future orbital hyperspectral sensors.

## Acknowledgments

The authors wish to acknowledge the support and instructive advice of Professor Yehuda Eyal and Dr. Onn Crouvi (Geological Survey of Israel), Mrs. Rachel Lugasi (Tel-Aviv University), and Dr. Natalia Panov (Jacob Blaustein Institutes) and to thank Mr. Alexander Goldberg and Mrs. Mazal Adar for helpful technical support.

## References

1. M. J. Abrams, R. P. Ashly, L. C. Rowan, A. F. H. Goetz, and A. B. Kahle, "Mapping of hydrothermal alteration in the Curprite Mining district, Nevada, using aircraft scanner imagery for the 0.46-2.36 mm spectral region," *Geology* **5**, 713–718 (1977).
2. G. R. Hunt, "Spectral signatures of particulate minerals, in the visible and near- infrared," *Geophysics* **42**, 501–513 (1977).
3. A. F. H. Goetz, B. N. Rock, and L. C. Rowan, "Remote sensing for exploration: An overview," *Econ. Geol.* **78**, 20–41 (1983).
4. R. N. Clark and T. L. Roush, "Reflectance spectroscopy: Quantitative analysis techniques for remote sensing applications," *J. Geophys. Res.* **89**(B7), 6329–6340 (1984).
5. F. A. Kruse, J. W. Boardman, and J. F. Huntington, "Comparison of airborne hyperspectral data and EO-1 Hyperion for mineral mapping," *IEEE Trans. Geosci. Remote Sens.* **41**(6), 1388–1400 (2003).
6. E. Ben-Dor and F. A. Kruse, "Surface mineral mapping of Makhtesh Ramon Negev, Israel using GER 63 channel scanner data," *Int. J. Remote Sens.* **16**(18), 3529–3553 (1995).
7. E. Ben-Dor, F. A. Kruse, A. B. Lefkoff, and A. Banin, "Comparison of three calibration techniqes for the utilization of GER 63 channel scannerdata of Makhtesh Ramon, Negev, Israel," *Photogramm. Eng. Remote Sens.* **60**, 1339–1354 (1994).
8. F. F. Sabins, "Remote sensing for mineral exploration," *Ore Geol. Rev.* **14**(3–4), 157–183 (1999).
9. C. Sabine, A. F. H. Goetz, L. Krosley, and H. W. Olsen, "Use of hyperspectral images in the identification and mapping of expansive clay soils and the role of spatial resolution," *Remote Sens. Environ.* **82**, 431–445 (2002).
10. F. Van Der Meer, "Imaging spectrometry for geological remote sensing," *Geologie En Mijnbouw-Netherlands J. Geosci.* **77**(2), 137–151 (1998).
11. F. Van Der Meer, "Can we map swelling clays with remote sensing?," *Int. J. Appl. Earth Obs. Geoinf.* **1**(3–4), 234–235 (1999).
12. B. Felzer, P. Hauff, and A. Goetz, "Quantitative reflectance spectroscopy of buddingtonite from the Cuprite mining district, Nevada," *J. Geophys. Res.* **99**(B2), 2887–2895 (1994).
13. M. A. Folkman, J. Pearlman, L. B. Liao, and P. J. Jarecke, "EO-1/Hyperion hyperspectral imager design, development, characterization, and calibration," *SPIE* **4151**, 40–51 (2001).
14. B. Datt, T. R. McVicar, T. G. Van Niel, D. L. B. Jupp, and J. S. Pearlman, "Preprocessing EO-1 Hyperion hyperspectral data to support the application of agricultural indexes," *IEEE Trans. Geosci. Remote Sens.* **41**(6), 1246–1259 (2003).
15. T. J. Cudahy, R. Hewson, J. F. Huntington, M. A. Quigley, and P. S. Barry, "The performance of the satellite-borne Hyperion Hyperspectral VNIR-SWIR imaging system for mineral mapping at Mount Fitton, South Australia," *IEEE Trans. Geosci. Remote Sens.* **41**(6), 9–13 (2001).

16. G. P. Asner and K. B. Heidebrecht, "Imaging spectroscopy for desertification studies: Comparing AVIRIS and EO-1 Hyperion in Argentina drylands," *IEEE Trans. Geosci. Remote Sens.* **41**(6), 1283–1296 (2003).
17. R. O. Green, B. E. Pavri, and T. G. Chrien, "On-orbit radiometric and spectral calibration characteristics of EO-1 Hyperion derived with an underflight of AVIRIS and *in situ* measurements at Salar de Arizaro, Argentina," *IEEE Trans. Geosci. Remote Sens.* **41**(6), 1194–1203 (2003).
18. R. Gersman, E. Ben-Dor, M. Beyth, D. Avigad, M. Abraha, and A. Kibreab, "Mapping of hydrothermally altered rocks by the EO-1 Hyperion sensor, Northern Danakil Depression, Eritrea," *Int. J. Remote Sens.* **29**(13), 3911–3936 (2008).
19. X. Zhang and P. Micha, "Comparison of lithologic mapping with ASTER, hyperion, and ETM data in the southeastern Chocolate Mountains, USA," *Photogramm. Eng. Remote Sens.* **73**(5), 555–561 (2007).
20. J. Wang, Y. Chen, T. He, C. Lv, and A. Liu, "Application of geographic image cognition approach in land type classification using Hyperion image: A case study in China," *Int. J. Appl. Earth Obs. Geoinf.* **12**(Suppl. 2), S212–S222 (2010).
21. C. Spinetti, F. Mazzarini, R. Casacchia, L. Colini, M. Neri, B. Behncke, R. Salvatori, M. F. Buongiorno, and M. T. Pareschi, "Spectral properties of volcanic materials from hyperspectral field and satellite data compared with LiDAR data at Mt. Etna," *Int. J. Appl. Earth Obs. Geoinf.* **11**(2), 142–155 (2009).
22. F. A. Kruse, J. W. Boardman, and J. F. Huntington, "Comparison of EO-1 Hyperion and airborne hyperspectral remote sensing data for geologic applications," *IEEE Trans. Geosci. Remote Sens.* **41**, 1388–1400 (2002).
23. B. E. Hubbard, J. K. Crowley, and D. R. Zimbelman, "Comparative alteration mineral mapping using visible to shortwave infrared (0.4–2.4 mu m) Hyperion, ALI, and ASTER imagery," *IEEE Trans. Geosci. Remote Sens.* **41**(6), 1401–1410 (2003).
24. Y. Eyal and Z. Rehes, "Tectonic analysis of the Dead Sea rift region sins the late cretaceous based on mesostructures," *Tectonics* **2**, 167–185 (1983).
25. R. Freund, I. Zak, and Z. Garfunkel, "Age and Rate of the sinistral movement along the Dead Sea rift," *Nature* **220**(5164), 253–255 (1968).
26. A. S. Al-Zoubi and E. Salameh, "A new evidence for lateral displacement along Wadi Araba Fault/ the Dead Sea Transform, Jordan," *Pakistan J. Appl. Sci.* **3**(4), 216–224 (2003).
27. M. Beyth, J. Henkel, and R. Geerken, *Applying Image Processing Technique and Reflectance Measurements Combined with Detailed Field Work for Analyzing TM Data of an Arid Area, Southern Israel*, Geological Survey of Israel, Vol. **11** (1998).
28. M. Atallah, "*Application of Remote Sensing and Field Techniques to Tectonic Problems of the Dead Sea Rift in Jordan*," Technischen University, Munchen (1986).
29. I. Rabb'a, "The geology of the Al Qurayqira (Jabal Hamra Faddan): Map Sheet No 3051 II. Amman," 1994.
30. G. Abdelhamid and I. Rabba, "An investigation of mineralized zones revealed during geological mapping, Jabal Hamra Faddan & Wadi Araba, Jordan, using LandsatTM data," *Int. J. Remote Sens.* **15**(7), 1495–1506 (1994).
31. M. Beyth, "Mineralizations related to Rift systems: Examples from the Gulf of Suez and the Dead Sea Rift," *Tectonophysics* **141**, 191–197 (1987).
32. B. Rothenberg, "Research in the southern Aravah 1959–1990 sumery of thirty years of archeao-metallurgical field work in the Timna Valley, the Wadi Amram and the southern Arabah (Israel)," *ISSN* **2-3**, 5–42 (1997).
33. F. Bender, *Geology of Jordan, Contribution to the Geology of the World*, Berlin, P.P. 196 (1974).
34. S. J. McLaren, D. D. Gilbertson, J. P. Grattan, C. O. Hunt, G. A. T. Duller, and G. A. Barker, "Quaternary palaeogeomorphologic evolution of the Wadi Faynan area, southern Jordan," *Palaeogeogr., Palaeoclimatol., Palaeoecol.* **205**(1–2), 131–154 (2004).

35. G. Barker, O. H. Creighton, D. Gilbertson, C. Hunt, S. McLaren, D. Mattingly, and D. C. Thomas, "The Wadi Faynan Project, Southern Jordan: A preliminary report on geomorphology and landscape archaeology," *Levant* **29**, 19–41 (1997).
36. H. Kaufmann, "Mineral exploration along the Aqaba-Levant structure by use of TM-data–Concepts, processing and results," *Int. J. Remote Sens.* **9**, 1639–1658 (1988).
37. R. D. Fiete and T. Tantalo, "Comparison of SNR image quality metrics for remote sensing systems," *Opt. Eng.* **40**(4), 574–585 (2001).
38. B.-C. Gao, "An operational method for estimating signal to noise ratios from data acquired with imaging spectrometers," *Remote Sens. Environ.* **43**(1), 23–33 (1993).
39. K. Staenz, R. A. Neville, S. Clavette, R. Landry, and H. P. White, "Retrieval of Surface Reflectance from Hyperion Radiance Data," *IEEE Geosc. Remote Sensing Lett.* **1**(2), 1419–1421 (2002).
40. R. O. Green, "Spectral calibration requirement for earth-looking imaging spectrometers in the solar-reflected spectrum," *Appl. Opt.* **37**, 683– 690 (1998).
41. A. Dadon, E. Ben-Dor, and A. Karnieli, "Use of derivative calculations and minimum noise fraction transform for detecting and correcting the spectral curvature effect (smile) in Hyperion images," *IEEE Trans. Geosci. Remote Sens.* **48**(6), 2603–2612 (2010).
42. A. Berk, L. S. Bernstein, G. P. Anderson, P. K. Acharya, D. C. Robertson, J. H. Chetwynd, and S. M. Adler-Golden, "MODTRAN cloud and multiple scattering upgrades with application to AVIRIS," *Remote Sens. Environ.* **65**(3), 367–375 (1998).
43. R. O. Green (2001). Atmospheric Correction Now (ACORN), developed by ImSpec LLC, available from Analytical Imaging and Geophysics LLC.
44. ASD–Analytical Spectral Devices Inc., tutorial, misc.asp. http://www.asdi.com/faq (1990).
45. G. M. Smith and E. J. Milton, "The use of the empirical line method to calibrate remotely sensed data to reflectance," *Int. J. Remote Sens.* **20**(13), 2653–2662 (1999).
46. N. Fujimoto, Y. Takahashi, T. Moriyama, M. Shimada, H. Wakabayashi, Y. Nakatani, and S. Obayashi, "Evaluation of SPOT HRV image data received in Japan," in *IGARSS '89 and Canadian Symposium on Remote Sensing, 12th, Vancouver, Canada*, pp. 463–466 (1989).
47. F. A. Kruse, A. B. Lefkoff, J. W. Boardman, K. B. Heidebrecht, A. T. Shapiro, P. J. Barloon, and A. F. H. Goetz, "The spectral image-processing system (SIPS)–interactive visualization and analysis of imaging spectrometer data," *Remote Sens. Environ.* **44**(2–3), 145–163 (1993).
48. P. Debba, F. J. A. van Ruitenbeek, F. D. Van Der Meer, E. J. M. Carranza, and A. Stein, "Optimal field sampling for targeting minerals using hyperspectral data," *Remote Sens. Environ.* **99**(4), 373–386 (2005).
49. F. Van Der Meer, "The effectiveness of spectral similarity measures for the analysis of hyperspectral imagery," *Int. J. Appl. Earth Obs. Geoinf.* **8**(1), 3–17 (2006).
50. A. P. Crosta, C. Sabine, and J. V. Taranik, "Hydrothermal alteration mapping at Bodie, California, using AVIRIS hyperspectral data," *Remote Sens. Environ.* **65**(3), 309–319 (1998).
51. R. E. Jensen and R. W. Spencer, "Matrix scaling of subjective probabilities of economic forecasts," *Econ. Lett.* **20**(3), 221–225 (1986).
52. A. Liu, P. Frazier, and L. Kumar, "Comparative assessment of the measures of thematic classification accuracy," *Remote Sens.Environ.* **107**(4), 606–616 (2007).
53. R. G. Congalton, "A review of assessing the accuracy of classifications of remotely sensed data, remote sensing of environment," *Remote Sens. Environ.* **37**, 35–46 (1991).
54. I. Cohen, "A coefficient of agreement for nominal scales," *Educ. Psychol. Meas.* **20**, 37–46 (1960).

**Alon Dadon** received his BSc degree in geology and environmental sciences from the Ben-Gurion University of the Negev, Beer–Sheva, Israel in 2004 and his MSc degree (Cum Laude) from Ben-Gurion University of the Negev, at the Jacob Blaustein Institutes for Desert Research department of Solar Energy and Environmental Physics, Sede Boqer, Israel, in 2006, where he is currently conducting a PhD research. He is a member of the hyperspectral specialist group of the Israeli ministry of science and Israeli space agency. He was awarded the "Ilan Ramon fellowship" of the Israeli ministry of science for a period of three years. His research interests are mainly satellite and surface-based hyperspectral remote sensing, focusing on imaging spectroscopy preprocessing and data analysis for geological applications.

**Eyal Ben-Dor** is a professor at the Tel Aviv University (TAU). He served as the chairman of the Geography and Human Environment Department at TAU from 2005 to 2009. He is currently the head of the Remote Sensing Laboratory within this department. He has more than 20 years of experience in remote sensing of the Earth with a special emphasis on imaging spectroscopy technology and soil spectroscopy. He received his PhD from the Hebrew University of Jerusalem, Faculty of Agriculture in Soil Science in 1992 and conducted a post doc fellowship in Center of Study the Earth from Space, University of Colorado at Boulder from 1992 to 1994. His studies focus on both quantitative and qualitative analyses of field and laboratory reflectance data and on processing of airborne and orbital hyper spectroscopy data for precise and advanced surface and atmosphere mapping of the environment.

**Michael Beyth** received his BSc and MSc degrees in geology from the Hebrew University, Jerusalem and in 1972 received his Dr. rer. nat. degree in geology from the University of Bonn, Germany. His main fields of interest are sustainable development of natural resources research and development and policy; energy policy and research and development for renewable and conservation. He worked in Israel, Ethiopia, Eritrea, Germany, USA, Brazil, Jordan, and Sinai and held main positions such as director of the Geophysical Institute, Israel; director of the Earth Science Research Administration, Israel; chief scientist of Ministry of National Infrastructures, Israel; head of mapping team in Ethiopia; and president of the Geological Society, Israel. He is currently a full professor emeritus in the Geological Survey of Israel.

**Arnon Karnieli** received his PhD from the University of Arizona in 1988 and since then has served as the head of the Remote Sensing Laboratory of the Jacob Blaustein Institutes for Desert Research, Ben Gurion University of the Negev. His main research interests are focused on processing of spaceborne, airborne, and ground spectroscopic data of drylands with respect to desertification and climate change processes. He is the Israeli principle investigator of the forthcoming Vegetation and Environmental New Micro Spacecraft (VEN$\mu$S) mission.